

Gaussian-to-Non-Gaussian Transition of a Quantum Spin Bath Revealed by Fourth-Order Correlation

Fan Xia^{1,2}, Shuowei Li,³ Xin-Yu Pan,^{1,2,4} Ping Wang,^{3,*} and Gang-Qin Liu^{1,2,4,†}

¹Beijing National Laboratory for Condensed Matter Physics, *Institute of Physics, Chinese Academy of Sciences, Beijing 100190, China*

²School of Physical Science, *University of Chinese Academy of Sciences, Beijing 100049, China*

³Faculty of Arts and Sciences, *Beijing Normal University, Zhuhai 519087, China*

⁴CAS Center of Excellence in Topological Quantum Computation, *University of Chinese Academy of Sciences, Beijing 100190, China*

 (Received 25 January 2025; revised 16 April 2025; accepted 27 May 2025; published 23 June 2025)

Non-Gaussian fluctuations are one of the essential properties of quantum systems. However, the direct detection of non-Gaussian fluctuations has not yet been achieved in experiments since the specific order of correlation has to be isolated from the complex dynamics of the whole system. In this Letter, we measure the second- and fourth-order correlations of ¹³C nuclear spins around a nitrogen vacancy center in diamond, using the recently developed quantum nonlinear spectroscopy. By adjusting the detection window and the spectral resolution, we observe the Gaussian to non-Gaussian transition of the multispin system. We find that the fourth-order correlation provides a fingerprint signal that can be used to identify individual spins with the same precession frequency, suggesting that Gaussianity is a potential quantum resource for quantum sensing. Our results shed light on the study of nonequilibrium quantum many-body dynamics and quantum materials at the nanoscale.

DOI: [10.1103/4fdk-dblq](https://doi.org/10.1103/4fdk-dblq)

Quantum fluctuations play a fundamental role in quantum field theory [1], quantum statistical physics [2], and quantum phase transition [3], which form the basis for understanding the equilibrium and nonequilibrium properties of quantum systems. In an ideal quantum system exhibiting Gaussian properties, the second-order correlation is sufficient for describing the dynamics of the entire system, as Wick's theorem states. However, realistic quantum systems usually exhibit non-Gaussian properties that go beyond the second-order correlation, and therefore the high-order correlations contain indispensable information to describe them. In particular, high-order correlations in quantum system are closely related to nonequilibrium quantum many body dynamics [4,5], quantum critical phenomena [6–9], and quantum information science [10–12].

Although high-order quantum fluctuations are widely used in theoretical analysis and calculations [1,2], the experimental measurement of these fluctuations is not an easy task [13]. For the spatial degree of freedom, high-order correlations have been experimentally characterized in the cold atom system [4,5,14]. However, in the time domain, conventional methods such as the widely used noise spectrum [15,16] and correlation measurements can only measure the second-order correlation [17–25] or detect the high-order correlations in a mixed form [26], which hinders the investigation of non-Gaussianity in realistic quantum

systems. The isolation of arbitrary types and orders of correlations has only recently become possible, after the development of quantum nonlinear spectroscopy [27,28] and experimental demonstration in the NMR system [28]. These advances enable the quantitative characterization of non-Gaussianity in realistic quantum systems.

In this Letter, we focus on the experimental isolation of the fourth time-ordered correlations (TOCs) of a realistic quantum environment, in particular the ¹³C nuclear spins around a nitrogen vacancy (NV) center in diamond. We demonstrate that the two-dimensional spectral feature of the fourth-order fluctuation is a unique indicator of the non-Gaussian feature of the multispin system. The selectivity and robustness of the quantum channel method [28] is significantly improved by integrating it with the dynamical decoupling (DD) technique. The number of nuclear spins involved is tuned by choosing DD sequences with different pulse numbers, which enables the observation of a transition between non-Gaussian and Gaussian features of the quantum spin bath. Moreover, we find that the non-Gaussian feature can serve as a fingerprint signal to identify the existence of a single spin, which is important for the single-molecule magnetic resonance technique [29].

In our experiment, the electron spin of an NV center in diamond serves as a local quantum probe, and the nearby ¹³C forms the multispin system, as shown in Fig. 1(a). Under periodic control of the NV probe, the nuclear spins and the NV electron spin are coupled via an effective coupling (in the interaction picture) [22,26]:

*Contact author: wpking@bnu.edu.cn

†Contact author: gqliu@iphy.ac.cn

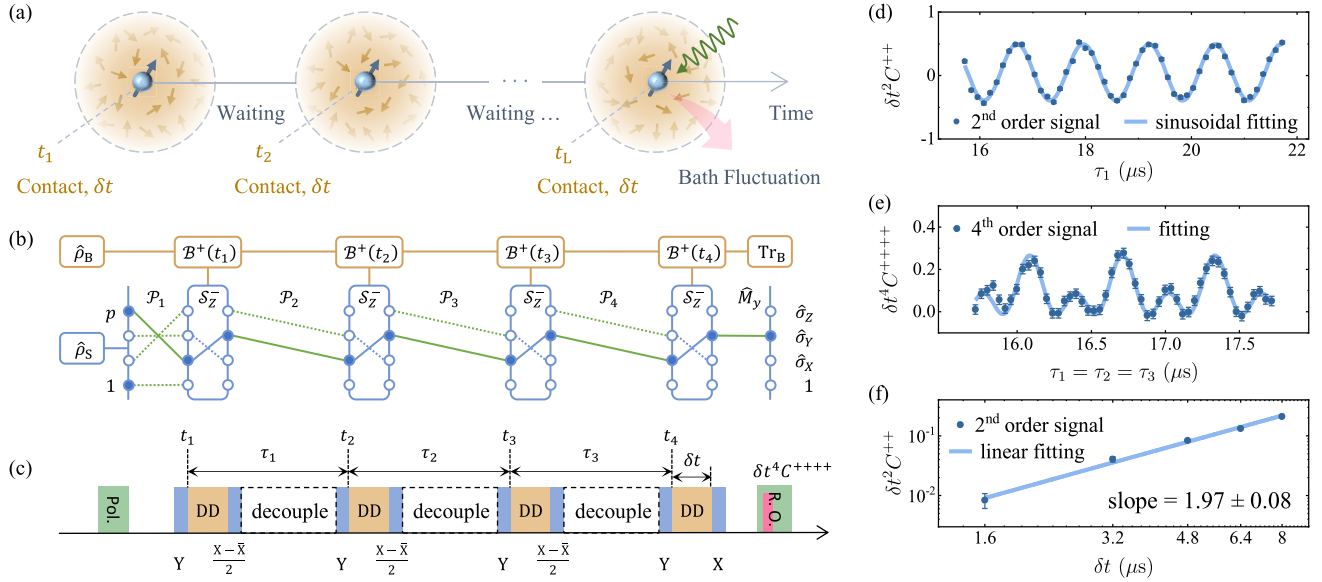


FIG. 1. Non-Gaussian fluctuation revealed by high-order correlation measurement. (a) Schematic illustration of measuring the L th time-ordered correlations of a ^{13}C nuclear spin bath surrounding an NV center (blue arrow) in diamond. The sensor interacts with the target at time points t_i , each for a short duration δt . (b) Quantum channels for extracting the fourth-order correlation C^{++++} . The quantum channel scheme is represented graphically in the basis of Pauli 4-operators. The solid lines represent the selected path to measure the correlations of interest, and the dashed lines show blocked paths. The quantum channel is constructed as $\mathcal{P}_1 = \mathcal{R}_y(\pi/2)$, $\mathcal{P}_2 = \mathcal{P}_3 = \mathcal{P}_4 = \mathcal{R}_y(\pi/2)[\mathcal{R}_x(\pi/2) - \mathcal{R}_{-x}(\pi/2)]/2$, which is synthesized by different rotations. Here the $\mathcal{R}_y(\pi/2)$ is used to transfer the signal to the channel with a long relaxation time to ensure high spectral resolution. (c) Experimental implementation of the quantum channels shown in (b). The waiting time is defined as $\tau_i = t_{i+1} - t_i$. (d) Second-order and (e) fourth-order correlation signals of an artificial monochromatic AC field with uniformly randomized phase, measured as a function of the waiting time τ_1 and $\tau_1 = \tau_2 = \tau_3$, respectively. (f) The amplitude of $\delta t^2 C^{++}$ versus the interaction interval δt .

$$\hat{V}(t) = \hat{S}_z \hat{B}(t), \quad (1)$$

where \hat{S}_z is the z component of the spin operator of the sensor and $\hat{B}(t) = e^{i\hat{H}_B t} \hat{B} e^{-i\hat{H}_B t}$ is the time dependent quantum noise operator of the nuclear spins. Here $\hat{B} = \sum_{i=1}^N A_{i,\perp} \hat{I}_{i,x}$ with $A_{i,\perp}$ denoting effective hyperfine coupling to the i th nuclear spin \hat{I}_i , and the bath Hamiltonian $\hat{H}_B = \sum_{i=1}^N \omega_i \hat{I}_{i,z}$ contains the Zeeman splitting of N nuclear spins with ω_i denoting the modified Larmor frequency by hyperfine coupling [22,26]. The nuclear spin bath is in the infinite high-temperature state $\hat{\rho}_B = 1/2^N$. Since $\hat{B}(t)$ is an operator, the classical correspondence of the L th order fluctuation cannot be directly formulated as the expectation value of the product of operators at different times [25,30]. Instead, it should be symmetrized to [27,28,31]

$$C^{++++}(t_L, \dots, t_2, t_1) = \text{Tr}_B[\mathcal{B}^+(t_L) \cdots \mathcal{B}^+(t_2) \mathcal{B}^+(t_1) \hat{\rho}_B], \quad (2)$$

through the definition of superoperator $\mathcal{B}^+(t) \hat{\rho} \equiv \{\hat{B}(t), \hat{\rho}\}/2$ constructed by anticommutator.

To selectively detect the L th order fluctuation in Eq. (2), the sensor spin is first prepared in the state $\hat{\rho}_S = (1 + \hat{\sigma}_z)/2$

and then interacts with the target L times for a short duration δt (contact time) to measure the L th order TOCs [Fig. 1(a)]. In order to isolate the desired TOCs, L quantum channels \mathcal{P}_i (a superoperator realized by combining different unitary controls) are inserted between these contacts. Finally, the observable $\hat{\sigma}_y$ of the sensor is measured, yielding the outcome $\delta t^L C^{++++}$. For the cases discussed here, C^{++++} is selected by the quantum channels designed in Fig. 1(b), and C^{++} is detected by quantum channels shown in Fig. S1. The experimental implementation is carried out using the sequence shown in Fig. 1(c). Green laser pulses are used to polarize and read out the NV spin state, while resonant microwave pulses are used to control the NV spin state and construct the designed quantum channels [indicated by blue blocks in Fig. 1(c)]. At each contact, a DD sequence is applied to the probe to adjust the detection frequency, enabling the accumulation of target information via the coupling described in Eq. (1). During the waiting time between contacts, defined as $\tau_i = t_{i+1} - t_i$, nonresonant DD sequences are applied to decouple the probe from the nuclear spins, thereby allowing the quantum bath to evolve freely. The longest free evolution time determines the spectral resolution of the correlation measurement.

We first calibrate the protocol by using it to detect an artificial AC field with a uniformly distributed random

phase. Both the second-order fluctuation $C^{++}(\tau_1)$ and the fourth-order $C^{++++}(\tau_1 = \tau_2 = \tau_3)$ of the AC field are measured for short δt , as shown in Figs. 1(d) and 1(e). C^{++} of the AC field shows a sinusoidal oscillation signal that agrees well with the theoretical prediction $C^{++} \propto \cos(\omega_0\tau_1)$. Figure 1(f) shows the amplitude of the second-order signal as a function of δt . The observed scaling is close to the ideal scaling δt^2 , which confirms the short time condition [27,28] and thus guarantees the correct reconstruction of the TOCs. We find that both C^{++} and C^{++++} can be fitted with the same parameters using the analytical formula of the correlations of the AC signal $C^{++++} \propto [1 + \cos(2\omega_0\tau_1) + \cos(4\omega_0\tau_1)]$, see Supplemental Material [32], Note 3 for more details. These results confirm that the quantum channel protocol can accurately extract both the second- and fourth-order correlations with the single-spin probe.

For the nuclear spin bath, the fourth-order fluctuation can be decomposed into Gaussian and non-Gaussian contributions as follows:

$$\begin{aligned}
 C^{++++} &= \text{Gaussian Pairings} \\
 &- \sum_{i=1}^N C_i^{++}(t_3, t_1) C_i^{++}(t_4, t_2) \\
 &- \sum_{i=1}^N C_i^{++}(t_4, t_1) C_i^{++}(t_3, t_2), \quad (3)
 \end{aligned}$$

where *Gaussian Pairings* $\equiv C^{++}(t_2, t_1)C^{++}(t_4, t_3) + C^{++}(t_3, t_1)C^{++}(t_4, t_2) + C^{++}(t_4, t_1)C^{++}(t_3, t_2)$ denotes the Gaussian terms that originate from the Wick factorization and the other terms represent the non-Gaussian contribution (Supplemental Material [32], Note 5). Non-negligible non-Gaussian terms will evidently contribute to the fourth-order fluctuation and consequently influence its spectral features.

We use the spectral feature of fourth-order correlation to characterize the non-Gaussian property of the ^{13}C nuclear spins around the NV center. Specifically, we investigate the 2D spectra of C^{++++} as a function of τ_1 and $\tau_2 = \tau_3$ (corresponding to ω' and ω after applying the FFT). In this case, the fourth-order correlation is expressed as follows (see Supplemental Material [32], Note 5 for more details):

$$\begin{aligned}
 C^{++++} &= \sum_{i_1, i_2=1}^N \sum_{s_1, s_2=-1, 1} \frac{A_{i_1, \perp}^2 A_{i_2, \perp}^2}{64} [e^{is_1\omega_{i_1}\tau_1} e^{is_2\omega_{i_2}\tau_2} \\
 &+ (1 - \delta_{i_1 i_2}) e^{is_1\omega_{i_1}\tau_1} e^{i(s_1\omega_{i_1} + 2s_2\omega_{i_2})\tau_2} \\
 &+ (1 - \delta_{i_1 i_2}) e^{is_1\omega_{i_1}\tau_1} e^{i(2s_1\omega_{i_1} + s_2\omega_{i_2})\tau_2}]. \quad (4)
 \end{aligned}$$

The terms relating to the Kronecker delta function $\delta_{i_1 i_2}$ result from the non-Gaussian correction in Eq. (3), and the others come from the Gaussian term. The non-Gaussian terms have the frequency components $\pm(\omega_i, 3\omega_i)$ and

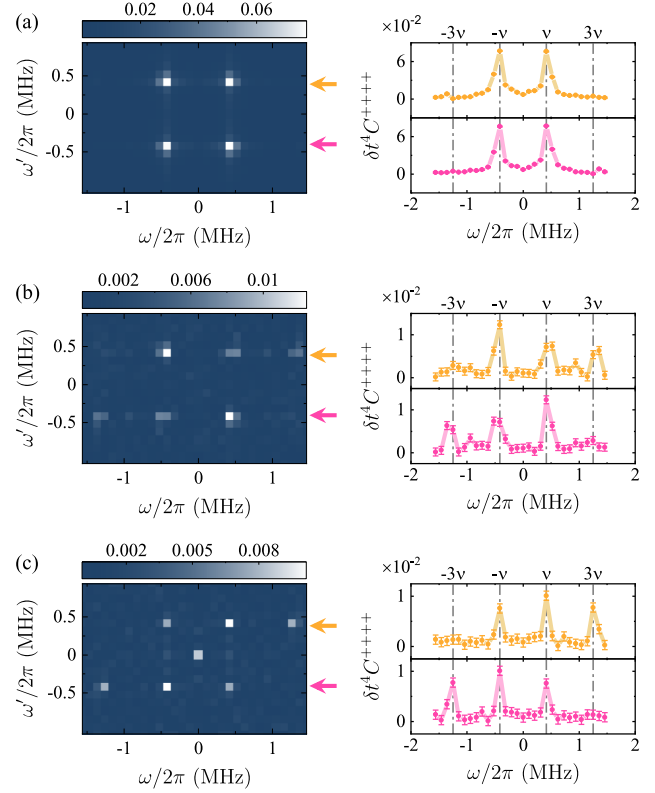


FIG. 2. Gaussian-to-non-Gaussian transition of the nuclear spin bath. 2D spectra of the fourth-order correlation are measured at different pulse numbers of the DD sequence N_p , which controls the detection window. The resolution of the spectra is low, so it can be assumed that all selected nuclear spins have the same precession frequency. (a) With the XY-16 sequence, only a single nuclear spin is included in the detection window, resulting in a spectrum with only four peaks and maximum non-Gaussianity. (b) With the XY-8 sequence, more nuclear spins are included, resulting in the appearance of two additional peaks at $\pm(\omega, 3\omega)$. (c) With the XY-4 sequence, the 2D spectrum shows six peaks with almost the same height, indicating the characteristic feature of the Gaussian bath. For all these cases, C^{++++} is measured as a function of τ_1 and τ_2 (with $\tau_3 = \tau_2$ fixed). The measurement is performed on a 20×30 pixel grid with a resolution of $2\pi \cdot 104.2$ kHz. The right panels show slices of the 2D spectra, as indicated by the arrows in the corresponding left panels. The error bars are 9.2×10^{-4} , 9.3×10^{-4} , and 9.2×10^{-4} from (a)–(c), respectively.

$\pm(\omega_i, \pm\omega_i)$. If this non-Gaussian contribution cannot be neglected, the delta function term can modify the ratio between the strength of the peaks $\pm(\omega_i, 3\omega_i)$ and $\pm(\omega_i, \pm\omega_i)$, thereby affecting the spectral structure of C^{++++} . In the following, we will discuss the spectral features of C^{++++} under different cases.

An interesting phenomenon in the multispin system is that its non-Gaussianity depends on the number of spins involved. In the simplest case, when only one nuclear spin is involved, the quantum nature of the single spin entails the strongest non-Gaussianity. This can be verified

experimentally by choosing a sharp filter function during the contact time. As shown in Fig. 2(a), a 4-peak pattern is observed when a DD sequence with $N_p = 16$ π -pulses (XY-16) is applied. These peaks are located at the positions $\pm(\omega, \pm\omega)$, in agreement with theoretical predictions. Next, we expand the detection window by reducing N_p while maintaining the low spectral resolution so that the frequency differences between the nuclear spins cannot be resolved. Under these circumstances, these nuclear spins can be treated as having the same frequency $\omega_i = \omega$. With $N_p = 8$ and 4, more nuclear spins are involved, resulting in six peaks in the 2D correlation spectra [Figs. 2(b) and 2(c)]. The two additional peaks are located at $\pm(\omega, 3\omega)$, as predicted by Eq. (4) when $\omega_i = \omega$. The non-Gaussian to Gaussian transition can be clearly resolved in the slices of the 2D spectra when N_p decreases from 16 to 4, as shown on the right side of Fig. 2.

To quantify this transition, we define a quantity η so that $1 - \eta$ represents the ratio between the strength of the peaks at $\pm(\omega, 3\omega)$ and $\pm(\omega, \pm\omega)$:

$$\eta = \frac{\overline{A^4}}{2N(\overline{A^2})^2 - \overline{A^4}}, \quad (5)$$

which follows from Eq. (4) for $\omega_i = \omega$ and reflects the degree of non-Gaussianity. Here $\overline{A^2} = \sum_{i=1}^N A_{i,\perp}^2 / N$ and $\overline{A^4} = \sum_{i=1}^N A_{i,\perp}^4 / N$ are the second and fourth moments of the coupling constant, respectively. For $N = 1$, we have $\eta = 1$ and the disappearance of peaks at $\pm(\omega, 3\omega)$, indicating maximum non-Gaussianity. In contrast, when $N \rightarrow \infty$, $\eta \rightarrow 0$ and the Gaussian pattern featuring six peaks of equal height emerges, indicating minimal non-Gaussianity. We calculate $\eta = 0.943, 0.448$, and 0.123 for the data shown in Figs. 2(a)–2(c), respectively, which clearly indicates the transition from a non-Gaussian to a Gaussian system.

The non-Gaussianity of the spin system can also be tuned by adjusting the spectral resolution. To demonstrate this in the experiment, we choose the duration of the XY-4 sequence so that four nuclear spins are included in the detection window. At a low resolution of $2\pi \times 104.2$ kHz, it is not possible to resolve different nuclear spins, and there would be six peaks, which is consistent with the Gaussian feature (Fig. S4). With increasing spectral resolution, a total of $4N(3N - 2)$ peaks can be resolved if all Larmor frequencies of the nuclear spins are distinguishable, as given by Eq. (4). An important feature is that the non-Gaussian terms in Eq. (3) will correct the relative height of the characteristic peaks $\pm(\omega_i, 3\omega_i)$, which result from the contribution of the isonuclear spins process [i.e., the Kronecker delta function in Eq. (4)]. In Fig. 3, as the resolution reaches $2\pi \times 15.625$ kHz, it is sufficient for resolving a strongly coupled nuclear spin with $\omega_1 = 2\pi \times 456.6$ kHz from the other three nuclear spins (with frequency of 415.8 kHz to 426.4 kHz). In this case, the

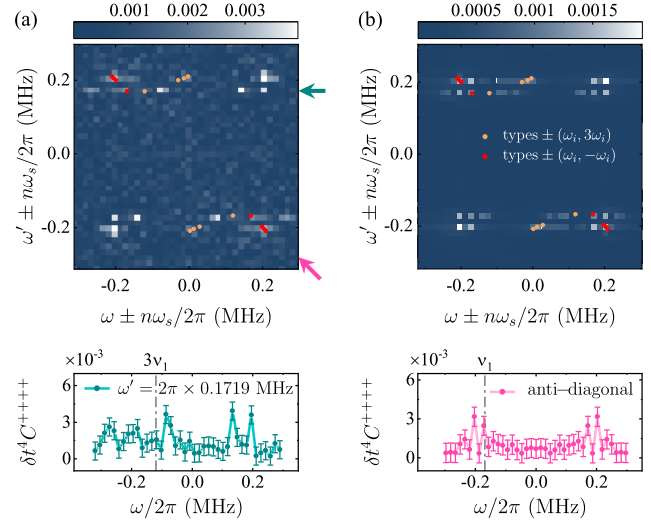


FIG. 3. 2D spectra of C^{++++} with high spectral resolution. (a) Experimental result. The pulse interval of the XY-4 sequence applied during contact is fixed at $1.275 \mu\text{s}$, which includes the four nuclear spins within the detection window. The red dots denote the peaks of types $\pm(\omega_i, -\omega_i)$ originating from these four nuclear spins, and the orange dots mark the corresponding peaks at $\pm(\omega_i, 3\omega_i)$. The under-sampling technique is used to increase the spectral resolution to $2\pi \cdot 15.625$ kHz with a 40×40 pixels grid. Due to the frequency ambiguity caused by the under sampling technique, the 2D spectrum is plotted in the first Brillouin zone, with a period $\omega_s = 2\pi \times 625.0$ kHz. (b) Numerical results. The 2D spectrum is derived using the hyperfine parameters measured in experiments. (a) and (b) use the same sampling parameters. The diagrams at the bottom show the slices indicated by the arrows. The peak at $3\omega_1$ disappears in the left plot, indicating the non-Gaussian feature of the nuclear spin bath. The error bar is 7.4×10^{-4} .

non-Gaussian term is sufficient to cancel the Gaussian term at the frequency $\pm(\omega_1, 3\omega_1)$, which leads to the disappearance of this peak. This feature is also clearly visible in the slice map, as can be seen in the bottom of Fig. 3. It is worth noting that the remaining peaks arise from pairings between different nuclear spins, and therefore only the $\pm(\omega, 3\omega)$ can be considered as a characteristic peak for the identification of non-Gaussianity.

The technique for detecting non-Gaussian fluctuations can be used to identify individual nuclear or electron spin [29,40], which is the key to single-molecule magnetic resonance [23,41,42]. To date, there is no “smoking-gun” method to distinguish a single spin from multiple spins with the same precession frequency, especially in scenarios with weak coupling or low spectral resolution (e.g., the case of a shallow NV center as a nanoscale quantum probe). In the present scheme, the disappearance of the characteristic peaks at $(\omega, 3\omega)$ of the 2D spectrum clearly proves that the frequency ω corresponds to a single nuclear spin. Furthermore, the analysis of the fourth-order correlations and their corresponding cumulants [10] provides insight

into the determination of different spin configurations or types of noise, such as two-spin clusters.

The fourth-order fluctuation C^{++++} measured here plays an important role in characterizing the non-Gaussian properties of quantum systems [43–45], which is crucial for optimal quantum control [11,28], fault-tolerant quantum computation, and other advanced quantum applications. For example, as shown in Fig. S6, the decoherence behavior of the central spin under the noisy AC field cannot be deduced from the measured second-order correlation alone. In this regard, the high-order fluctuations detected by our technique contain essential information for understanding and controlling realistic quantum systems. We would like to emphasize that this technique can be applied to most quantum systems, including color centers in SiC or hBN, spins in silicon, superconducting circuits, ions, and atomic qubits.

In summary, this study provides direct evidence of the Gaussian-to-non-Gaussian transition of a realistic multispin system in solid by detecting its fourth-order TOCs. We find that the 2D spectrum of the fourth-order TOCs can be used to unambiguously diagnose the non-Gaussianity of the nuclear spin system based on its characteristic peaks. The non-Gaussianity of the multispin system depends on both the detection window and the spectral resolution, or in other words, the time scale to be considered. In particular, the disappearance of the characteristic peak can be used to identify individual nuclear spins that are weakly coupled to the sensor, which could be useful in the context of nano-scale quantum sensing with a shallow NV center [46,47]. The method shown here paves the way for exploiting the non-Gaussian properties as a quantum resource for quantum sensing, which can be used to distinguish different quantum signals that behave the same in the second-order spectrum but completely different in the non-Gaussian spectrum.

In the near future, this technique can be used to characterize the non-Gaussian fluctuations induced by quantum many-body phenomena, such as the interplay between interaction and localization in quantum many-body systems or the competition between different symmetries in critical quantum systems [7,48–50], which are assumed to diverge near the critical point [6,9]. It can also be used to investigate the nonequilibrium quantum many-body dynamics of strongly interacted systems, such as the sine-Gordon model in cold atoms [4,5,14], and to probe the single-quanta excitation of nuclear spins around quantum dots [51,52] or in qubit-coupled magnon systems [53,54]. Furthermore, the detection of fourth-order correlation by a local probe allows us to develop a spatially [55–57] and temporally resolved high-order quantum spectroscopy that could provide multidimensional information and is therefore more powerful than conventional methods.

Acknowledgments—This work is supported by the Innovation Program for Quantum Science and Technology

(Grant No. 2023ZD0300600), the National Natural Science Foundation of China (Grants No. 12475012, No. 12074422, No. 12374468, No. T2121001, and No. 62461160263), the National Key Research and Development Program of China (Grant No. 2023YFA1608900), the Beijing Natural Science Foundation (Grants No. Z200009 and No. Z230005), the Guangdong Provincial Quantum Science Strategic Initiative (Grants No. GDZX2403009 and No. GDZX2303005), the Chinese Academy of Sciences (Grants No. YSBR-100 and No. XDB33000000).

Data availability—The data that support the findings of this Letter are openly available [58].

-
- [1] M. E. Peskin and D. V. Schroeder, *An Introduction To Quantum Field Theory* (Taylor Francis Ltd, London, 2019).
 - [2] M. Kardar, *Statistical Physics of Fields* (Cambridge University Press, Cambridge, England, 2010).
 - [3] S. Sachdev, *Quantum Phase Transitions* (Cambridge University Press, Cambridge, England, 2014).
 - [4] T. Schweigler, M. Gluza, M. Tajik, S. Sotiriadis, F. Cataldini, S.-C. Ji, F. S. Møller, J. Sabino, B. Rauer, J. Eisert, and J. Schmiedmayer, Decay and recurrence of non-Gaussian correlations in a quantum many-body system, *Nat. Phys.* **17**, 559 (2021).
 - [5] M. Prüfer, T. V. Zache, P. Kunkel, S. Lannig, A. Bonnin, H. Strobel, J. Berges, and M. K. Oberthaler, Experimental extraction of the quantum effective action for a non-equilibrium many-body system, *Nat. Phys.* **16**, 1012 (2020).
 - [6] S. Joubaud, A. Petrosyan, S. Ciliberto, and N. B. Garnier, Experimental evidence of non-Gaussian fluctuations near a critical point, *Phys. Rev. Lett.* **100**, 180601 (2008).
 - [7] A. Kremen, H. Khan, Y. L. Loh, T. I. Baturina, N. Trivedi, A. Frydman, and B. Kalisky, Imaging quantum fluctuations near criticality, *Nat. Phys.* **14**, 1205 (2018).
 - [8] F. Machado, E. A. Demler, N. Y. Yao, and S. Chatterjee, Quantum noise spectroscopy of dynamical critical phenomena, *Phys. Rev. Lett.* **131**, 070801 (2023).
 - [9] S. Borsányi, Z. Fodor, J. N. Guenther, S. D. Katz, P. Parotto, A. Pásztor, D. Pesznyák, K. K. Szabó, and C. H. Wong, Continuum-extrapolated high-order baryon fluctuations, *Phys. Rev. D* **110**, L011501 (2024).
 - [10] L. M. Norris, G. A. Paz-Silva, and L. Viola, Qubit noise spectroscopy for non-Gaussian dephasing environments, *Phys. Rev. Lett.* **116**, 150503 (2016).
 - [11] Y. Sung, F. Beaudoin, L. M. Norris, F. Yan, D. K. Kim, J. Y. Qiu, U. von Lüpke, J. L. Yoder, T. P. Orlando, S. Gustavsson, L. Viola, and W. D. Oliver, Non-Gaussian noise spectroscopy with a superconducting qubit sensor, *Nat. Commun.* **10**, 3715 (2019).
 - [12] S. Kotler, N. Akerman, Y. Glickman, and R. Ozeri, Non-linear single-spin spectrum analyzer, *Phys. Rev. Lett.* **110**, 110503 (2013).
 - [13] S. Paschen and Q. Si, Quantum phases driven by strong correlations, *Nat. Rev. Phys.* **3**, 9 (2021).

- [14] T. Schweigler, V. Kasper, S. Erne, I. Mazets, B. Rauer, F. Cataldini, T. Langen, T. Gasenzer, J. Berges, and J. Schmiedmayer, Experimental characterization of a quantum many-body system via higher-order correlations, *Nature (London)* **545**, 323 (2017).
- [15] G. A. Álvarez and D. Suter, Measuring the spectrum of colored noise by dynamical decoupling, *Phys. Rev. Lett.* **107**, 230501 (2011).
- [16] T. Fink and H. Bluhm, Noise spectroscopy using correlations of single-shot qubit readout, *Phys. Rev. Lett.* **110**, 010403 (2013).
- [17] A. Laraoui, F. Dolde, C. Burk, F. Reinhard, J. Wrachtrup, and C. A. Meriles, High-resolution correlation spectroscopy of ^{13}C spins near a nitrogen-vacancy centre in diamond, *Nat. Commun.* **4**, 1651 (2013).
- [18] S. Zaiser, T. Rendler, I. Jakobi, T. Wolf, S.-Y. Lee, S. Wagner, V. Bergholm, T. Schulte-Herbrüggen, P. Neumann, and J. Wrachtrup, Enhancing quantum sensing sensitivity by a quantum memory, *Nat. Commun.* **7**, 12279 (2016).
- [19] S. Schmitt, T. Gefen, F. M. Stürmer, T. Uden, G. Wolff, C. Müller, J. Scheuer, B. Naydenov, M. Markham, S. Pezzagna, J. Meijer, I. Schwarz, M. Plenio, A. Retzker, L. P. McGuinness, and F. Jelezko, Submillihertz magnetic spectroscopy performed with a nanoscale quantum sensor, *Science* **356**, 832 (2017).
- [20] N. Aslam, M. Pfender, P. Neumann, R. Reuter, A. Zappe, F. Fávoro de Oliveira, A. Denisenko, H. Sumiya, S. Onoda, J. Isoya, and J. Wrachtrup, Nanoscale nuclear magnetic resonance with chemical resolution, *Science* **357**, 67 (2017).
- [21] J. M. Boss, K. S. Cujia, J. Zopes, and C. L. Degen, Quantum sensing with arbitrary frequency resolution, *Science* **356**, 837 (2017).
- [22] M. Pfender, P. Wang, H. Sumiya, S. Onoda, W. Yang, D. B. R. Dasari, P. Neumann, X.-Y. Pan, J. Isoya, R.-B. Liu, and J. Wrachtrup, High-resolution spectroscopy of single nuclear spins via sequential weak measurements, *Nat. Commun.* **10**, 594 (2019).
- [23] K. S. Cujia, J. M. Boss, K. Herb, J. Zopes, and C. L. Degen, Tracking the precession of single nuclear spins by weak measurements, *Nature (London)* **571**, 230 (2019).
- [24] V. Vorobyov, S. Zaiser, N. Abt, J. Meinel, D. Dasari, P. Neumann, and J. Wrachtrup, Quantum fourier transform for nanoscale quantum sensing, *npj Quantum Inf.* **7**, 124 (2021).
- [25] Y. Shen, P. Wang, C. T. Cheung, J. Wrachtrup, R.-B. Liu, and S. Yang, Detection of quantum signals free of classical noise via quantum correlation, *Phys. Rev. Lett.* **130**, 070802 (2023).
- [26] J. Meinel, V. Vorobyov, P. Wang, B. Yavkin, M. Pfender, H. Sumiya, S. Onoda, J. Isoya, R.-B. Liu, and J. Wrachtrup, Quantum nonlinear spectroscopy of single nuclear spins, *Nat. Commun.* **13**, 5318 (2022).
- [27] P. Wang, C. Chen, X. Peng, J. Wrachtrup, and R.-B. Liu, Characterization of arbitrary-order correlations in quantum baths by weak measurement, *Phys. Rev. Lett.* **123**, 050603 (2019).
- [28] Z. Wu, P. Wang, T. Wang, Y. Li, R. Liu, Y. Chen, X. Peng, and R.-B. Liu, Selective detection of dynamics-complete set of correlations via quantum channels, *Phys. Rev. Lett.* **132**, 200802 (2024).
- [29] I. Lovchinsky, A. O. Sushkov, E. Urbach, N. P. de Leon, S. Choi, K. De Greve, R. Evans, R. Gertner, E. Bersin, C. Müller, L. McGuinness, F. Jelezko, R. L. Walsworth, H. Park, and M. D. Lukin, Nuclear magnetic resonance detection and spectroscopy of single proteins using quantum logic, *Science* **351**, 836 (2016).
- [30] P. Wang, C. Chen, and R.-B. Liu, Classical-noise-free sensing based on quantum correlation measurement, *Chin. Phys. Lett.* **38**, 010301 (2021).
- [31] G. Gasbarri and L. Ferialdi, Stochastic unravelings of non-Markovian completely positive and trace-preserving maps, *Phys. Rev. A* **98**, 042111 (2018).
- [32] See Supplemental Material at <http://link.aps.org/supplemental/10.1103/4fdk-dblq> for theoretical derivations and additional experimental details, including Refs. [33–39].
- [33] M. W. Doherty, N. B. Manson, P. Delaney, and L. C. L. Hollenberg, The negatively charged nitrogen vacancy centre in diamond: the electronic solution, *New J. Phys.* **13**, 025019 (2011).
- [34] M. W. Doherty, N. B. Manson, P. Delaney, F. Jelezko, J. Wrachtrup, and L. C. Hollenberg, The nitrogen-vacancy colour centre in diamond, *Phys. Rep.* **528**, 1 (2013).
- [35] G. de Lange, Z. H. Wang, D. Ristè, V. V. Dobrovitski, and R. Hanson, Universal dynamical decoupling of a single solid-state spin from a spin bath, *Science* **330**, 60 (2010).
- [36] W.-L. Ma and R.-B. Liu, Angstrom-resolution magnetic resonance imaging of single molecules via wave-function fingerprints of nuclear spins, *Phys. Rev. Appl.* **6**, 024019 (2016).
- [37] R. Kubo, Generalized cumulant expansion method, *J. Phys. Soc. Jpn.* **17**, 1100 (1962).
- [38] N. Zhao, S.-W. Ho, and R.-B. Liu, Decoherence and dynamical decoupling control of nitrogen vacancy center electron spins in nuclear spin baths, *Phys. Rev. B* **85**, 115303 (2012).
- [39] W. Yang, W.-L. Ma, and R.-B. Liu, Quantum many-body theory for electron spin decoherence in nanoscale nuclear spin baths, *Rep. Prog. Phys.* **80**, 016001 (2016).
- [40] F. Shi, Q. Zhang, P. Wang, H. Sun, J. Wang, X. Rong, M. Chen, C. Ju, F. Reinhard, H. Chen, J. Wrachtrup, J. Wang, and J. Du, Single-protein spin resonance spectroscopy under ambient conditions, *Science* **347**, 1135 (2015).
- [41] N. Zhao, J. Honert, B. Schmid, M. Klas, J. Isoya, M. Markham, D. Twitchen, F. Jelezko, R.-B. Liu, H. Fedder, and J. Wrachtrup, Sensing single remote nuclear spins, *Nat. Nanotechnol.* **7**, 657 (2012).
- [42] T. H. Taminiau, J. J. T. Wagenaar, T. van der Sar, F. Jelezko, V. V. Dobrovitski, and R. Hanson, Detection and control of individual nuclear spins using a weakly coupled electron spin, *Phys. Rev. Lett.* **109**, 137602 (2012).
- [43] L. Cywiński, W. M. Witzel, and S. Das Sarma, Pure quantum dephasing of a solid-state electron spin qubit in a large nuclear spin bath coupled by long-range hyperfine-mediated interactions, *Phys. Rev. B* **79**, 245314 (2009).
- [44] N. Zhao, Z.-Y. Wang, and R.-B. Liu, Anomalous decoherence effect in a quantum bath, *Phys. Rev. Lett.* **106**, 217205 (2011).
- [45] F. Reinhard, F. Shi, N. Zhao, F. Rempp, B. Naydenov, J. Meijer, L. T. Hall, L. Hollenberg, J. Du, R.-B. Liu, and J.

- Wrachtrup, Tuning a spin bath through the quantum-classical transition, *Phys. Rev. Lett.* **108**, 200402 (2012).
- [46] B. A. Myers, A. Das, M. C. Dartiailh, K. Ohno, D. D. Awschalom, and A. C. Bleszynski Jayich, Probing surface noise with depth-calibrated spins in diamond, *Phys. Rev. Lett.* **113**, 027602 (2014).
- [47] T. Rosskopf, A. Dussaux, K. Ohashi, M. Loretz, R. Schirhagl, H. Watanabe, S. Shikata, K. M. Itoh, and C. L. Degen, Investigation of surface magnetic noise by shallow spins in diamond, *Phys. Rev. Lett.* **112**, 147602 (2014).
- [48] S. Hsieh, P. Bhattacharyya, C. Zu, T. Mittiga, T. J. Smart, F. Machado, B. Kobrin, T. O. Höhn, N. Z. Rui, M. Kamrani, S. Chatterjee, S. Choi, M. Zaletel, V. V. Struzhkin, J. E. Moore, V. I. Levitas, R. Jeanloz, and N. Y. Yao, Imaging stress and magnetism at high pressures using a nanoscale quantum sensor, *Science* **366**, 1349 (2019).
- [49] F. Casola, T. van der Sar, and A. Yacoby, Probing condensed matter physics with magnetometry based on nitrogen-vacancy centres in diamond, *Nat. Rev. Mater.* **3**, 17088 (2018).
- [50] N. Wang, G.-Q. Liu, W.-H. Leong, H. Zeng, X. Feng, S.-H. Li, F. Dolde, H. Fedder, J. Wrachtrup, X.-D. Cui, S. Yang, Q. Li, and R.-B. Liu, Magnetic criticality enhanced hybrid nanodiamond thermometer under ambient conditions, *Phys. Rev. X* **8**, 011042 (2018).
- [51] D. A. Gangloff, G. Éthier Majcher, C. Lang, E. V. Denning, J. H. Bodey, D. M. Jackson, E. Clarke, M. Hugues, C. Le Gall, and M. Atatüre, Quantum interface of an electron and a nuclear ensemble, *Science* **364**, 62 (2019).
- [52] D. M. Jackson, D. A. Gangloff, J. H. Bodey, L. Zaporiski, C. Bachorz, E. Clarke, M. Hugues, C. Le Gall, and M. Atatüre, Quantum sensing of a coherent single spin excitation in a nuclear ensemble, *Nat. Phys.* **17**, 585 (2021).
- [53] D. Lachance-Quirion, S. P. Wolski, Y. Tabuchi, S. Kono, K. Usami, and Y. Nakamura, Entanglement-based single-shot detection of a single magnon with a superconducting qubit, *Science* **367**, 425 (2020).
- [54] D. Xu, X.-K. Gu, H.-K. Li, Y.-C. Weng, Y.-P. Wang, J. Li, H. Wang, S.-Y. Zhu, and J. Q. You, Quantum control of a single magnon in a macroscopic spin system, *Phys. Rev. Lett.* **130**, 193603 (2023).
- [55] J. Rovny, Z. Yuan, M. Fitzpatrick, A. I. Abdalla, L. Futamura, C. Fox, M. C. Cambria, S. Kolkowitz, and N. P. de Leon, Nanoscale covariance magnetometry with diamond quantum sensors, *Science* **378**, 1301 (2022).
- [56] W. Ji, Z. Liu, Y. Guo, Z. Hu, J. Zhou, S. Dai, Y. Chen, P. Yu, M. Wang, K. Xia, F. Shi, Y. Wang, and J. Du, Correlated sensing with a solid-state quantum multisensor system for atomic-scale structural analysis, *Nat. Photonics* **18**, 230 (2024).
- [57] T. Delord, R. Monge, and C. A. Meriles, Correlated spectroscopy of electric noise with color center clusters, *Nano Lett.* **24**, 6474 (2024).
- [58] G.-Q. Liu, Data for Gaussian to non-Gaussian transition of a quantum spin bath revealed by fourth-order correlation. Science Data Bank (2025), [10.57760/sciencedb.nbsdc.00227](https://doi.org/10.57760/sciencedb.nbsdc.00227).